Polymerized sp^2-sp^3 hybrid metallic phase of C_{60} as obtained via constant-pressure molecular dynamics

Yuichiro Yamagami and Susumu Saito
Department of Physics, Tokyo Institute of Technology, 2-12-1 Oh-okayama, Meguro-ku, Tokyo 152-8551, Japan
(Received 15 August 2008; revised manuscript received 16 December 2008; published 29 January 2009)

Using the tight-binding molecular-dynamics method, we study the pressure-induced structural phase transition of the two-dimensional "tetragonal" C_{60} polymer. It is found that the structural transition to a three-dimensionally (3D) polymerized C_{60} phase takes place for a wide range of pressure from 12 to 28 GPa. Although the lattice constants of this 3D polymer phase are close to those of experimentally observed values [S. Yamanaka *et al.*, Phys. Rev. Lett. **96**, 076602 (2006)], the present phase has much more sp^3 C sites than the experimentally proposed phase and each C_{60} has interfullerene chemical bonds with all the 12 neighbor C_{60} fullerenes. From the subsequent total-energy electronic-structure analysis in the framework of the density-functional theory, it is found that this completely polymerized C_{60} phase has much lower total energy than the previously proposed 3D polymer phases and possesses the metallic electronic structure.

DOI: 10.1103/PhysRevB.79.045425 PACS number(s): 61.48.−c, 71.20.Tx, 81.05.Tp

I. INTRODUCTION

Ever since the macroscopic production of C_{60} fullerenes[1] and the simultaneous discovery of solid C_{60} as a new phase of crystalline sp^2 carbon, the electronic and structural properties of molecular and solid phases of C_{60} have been studied extensively in many fields of science and engineering. It has been revealed theoretically[2] and experimentally[3] that the face-centered-cubic (fcc) solid C_{60} is semiconducting, while many kinds of alkali and/or alkaline-earth atom doping into the pristine phase can give rise to metallic[4] and even superconducting fullerides.[5,6] Doping metal atoms modifies the cohesive mechanism of C_{60} fullerenes in their solid phase from weak van der Waals type[2] to ionic cohesion with additional metallic cohesion. Another interesting way to modify the cohesive mechanism is the photoinduced and pressure-induced structural phase transition into polymerized C_{60} phases which possess interfullerene covalent bonds.[7,8]

Among various C_{60} polymer phases discussed so far, three phases identified by Xu and Scuseria[9] and Núñez-Regueiro *et al.*[10] are well known: the one-dimensional (1D) orthorhombic, the two-dimensional (2D) "tetragonal" (orthorhombic),[11] and the 2D rhombohedral phases. These C_{60} polymer phases have attracted many interests as new allotropes of carbon because of their low dimensionality and unprecedented sp^2-sp^3 hybrid crystalline geometry. On the other hand, they have also attracted interests as starting material for pressurization of nanostructured carbon since there should be many more stable crystalline C_{60} polymer phases including three-dimensional (3D) polymer-network phases to be synthesized. A variety of experimental and theoretical studies motivated by this idea were carried out,[12–14] and recently, an important experimental result on synthesis of a new polymer phase from the 2D orthorhombic phase via external pressure was reported.[15] The lattice constants with the body-centered-orthorhombic (bco) unit cell derived from the single-crystal x-ray structure analysis suggest that the product should be a 3D polymer. The importance of the starting material for producing new polymer phases has been clearly demonstrated by the experimental synthesis of another cubic polymer phase starting from the fcc solid C_{60} under the external pressure of 15 GPa.[16] It is the same external-pressure value as that applied to produce the interesting bco 3D polymer phase[15] from the 2D orthorhombic phase. Now the detailed geometries of this experimentally obtained polymerized phase and other possible 3D C_{60} polymer phases are of high interest.

Theoretically, the 3D polymer phase has been studied based on the static energetics, and several new crystalline phases have been found.[12,17] In the present work, in order to address this important issue in greater detail, we theoretically study the pressure-induced structural phase transition of the 2D orthorhombic polymer phase by using the tight-binding molecular-dynamics (TBMD) method. We study the structural stability and the phase transformation of the orthorhombic phase for a wide range of the external pressure, from 10 to 30 GPa. Interestingly, the new phases obtained via the TBMD simulations at various pressure values possess the bco or a nearly bco unit cell, with the completely polymerized C_{60} having interfullerene covalent bonds with all the 12 neighbor fullerenes. Using the local-density approximation (LDA) within the framework of the density-functional theory (DFT),[18,19] we also study the electronic structure and the total energy as well as the detailed geometries of the bco phase, which is the representative phase among several similar phases obtained via the TBMD simulations.

This paper is organized as follows. In Sec. II, the computational method used in this study as well as the system studied is given. In Sec. III, results of the TBMD simulation and the LDA study are given. In Sec. IV, this paper is summarized and concluded.

II. COMPUTATIONAL METHODS AND SYSTEM STUDIED

The molecular-dynamics (MD) method has been used frequently to study the structural phase transition of many kinds of materials at elevated temperature utilizing the Nosé thermostat.[20] The method has even revealed an interesting copolymerization of C_{60} and other molecules.[21] In the

present work, on the other hand, to study the structural phase transition under external pressure in the MD method, we use the scheme proposed by Parrinello and Rahman.[22] In this MD method, the shape and size of the MD cell vary so that the internal stress may balance with the external pressure. Therefore, in principle, this method can describe the pressure-induced structural phase transition that involves even the change of the periodicity of the system.

As for the total energy of the system as a function of the atomic geometry, we use the tight-binding (TB) method in order to avoid the self-consistent procedure which may require too much computational time to find the structural phase transition of nanostructured carbon materials in the MD process. In the TB method used in this study, the total energy is defined as follows:

$$E_{\mathrm{tot}} = E_{\mathrm{bs}} + E_{\mathrm{rep}}, \tag{1}$$

where E_{bs} is the band-structure energy to be given by the Hamiltonian matrix and E_{rep} is the short-range repulsive energy. In this method, we use the same functional forms as proposed by Xu *et al.*[23] to calculate the Hamiltonian matrix and E_{rep}. However, as for a parameter set to be used in the functional forms, we use the one proposed by Omata *et al.*[24] In this parameter set, the cutoff distance is as long as 7.0 Å which is much longer than the interlayer distance of graphite. Importantly, this parameter set has been so constructed that the TB energetics using it can reproduce the LDA energetics of not only the sp^2 (graphene) and sp^3 (diamond) covalent bonds but also that of the sp^2 interlayer interaction in both hypothetical *AA*- and realistic *AB*-stacked graphites. This sp^2 interlayer interaction is actually the interaction which governs the stability of the fcc C_{60} phase and 1D/2D C_{60} polymer phases, and, therefore, must be treated explicitly and accurately in predicting their structural phase transitions under pressure. Interestingly, the graphite interlayer distance is given rather accurately in LDA, while the generalized gradient approximation (GGA) even fails to give the finite interlayer distance of graphite.[25] It should be noted that the LDA energetics for graphite works well only when one considers a very fine mesh along the interlayer direction in the Brillouin-zone sampling. It is well known that both electron and hole Fermi surfaces appear along the interlayer direction at the zone boundary (K-H line) in graphite,[26–28] which may be the origin of the importance of a fine mesh in the Brillouin-zone sampling.

On the other hand, in the LDA total-energy electronic-structure calculation, the plane-wave basis set with a cutoff energy of 50 Ry and the norm-conserving pseudopotentials[29] with separable approximation[30] are used. As for the exchange-correlation functional, we adopt the Ceperley-Alder formula[31] parametrized by Perdew and Zunger.[32] The geometry optimization is performed by using the conjugate-gradient method.[33]

Using the TBMD method, we perform two kinds of simulations. We first perform the MD simulation under the external pressure (P_{ext}). The simulation is performed for various P_{ext} values: 10, 12, 14, 16, 18, 20, 22, 24, 26, 28, and 30 GPa. We adopt the "ground-state geometry" of the orthorhombic 2D polymer phase, i.e., the geometry optimized at

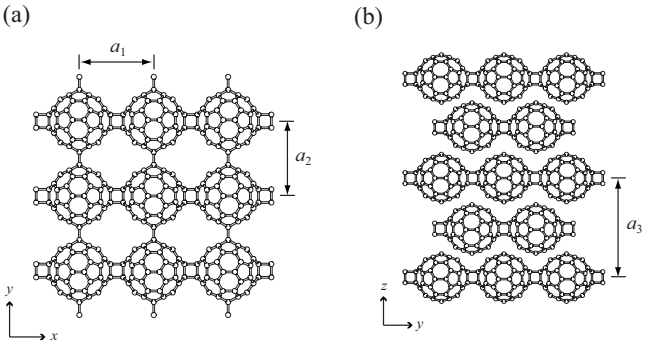

FIG. 1. Geometry of the "tetragonal" C_{60} polymer, which actually possesses the body-centered-orthorhombic unit cell. In this phase, C_{60} fullerenes form 2D covalent-bond network shown in (a), and these 2D network planes are stacked with the "*AB*" sequence shown in (b). Within a polymerized C_{60} plane, each C_{60} is connected to adjacent C_{60} fullerenes via a four-membered ring (the [2+2] cycloaddition-type bonding pattern) not only in the direction of the *x* axis but also in the direction of the *y* axis as is evident in (b).

$T=0$ (Fig. 1), as the initial geometry of the MD simulations. In order to search possible new phases with larger unit cell than that of the initial phase, we take the edges of the MD cell to be $\boldsymbol{a}_1=(a_1,0,0)$, $\boldsymbol{a}_2=(0,a_2,0)$, and $\boldsymbol{a}_3=(0,0,a_3)$, and independently treat two C_{60} fullerenes in the MD cell. The initial values of a_1, a_2, and a_3 are 8.82, 8.90, and 14.16 Å, respectively. With a time interval of 0.7256 fs, we carry out the simulation of each case for 2000 MD steps, which corresponds to 1.4512 ps. In our previous work, the various structural phase transitions have occurred within this simulation time for nanostructured carbon materials.[24] Therefore, this simulation time is to be long enough to search new phases in this study. The fictitious mass *W* in Ref. 22 used in the present simulation is 135 times the proton mass.[34]

When we obtain new phases under external pressure, we next examine their structural stabilities under ambient pressure and low temperature by using the following two ways. In one way, we first perform the geometry optimization for the final structure at 2000 MD steps with keeping the external pressure at initially applied value, and sequentially perform the geometry optimization again after setting the external (target) pressure to be zero. In the other way, we seamlessly continue the MD simulation for a while after switching the target pressure from P_{ext} to zero, and then perform the "cooling" simulation down to $T=0$. We call the former way as the way of "A," and the latter way as the way of "B."

In Fig. 2, we show the typical time evolution of T and p in the constant-pressure MD simulation, where T and p is temperature and internal pressure, respectively. In the constant-pressure molecular-dynamics method, the velocity of the *i*th particle is usually defined as follows:[22]

$$\boldsymbol{v}_i = \underline{h}\dot{\boldsymbol{s}}_i. \tag{2}$$

So in the present work, we regard the following quantity as temperature:

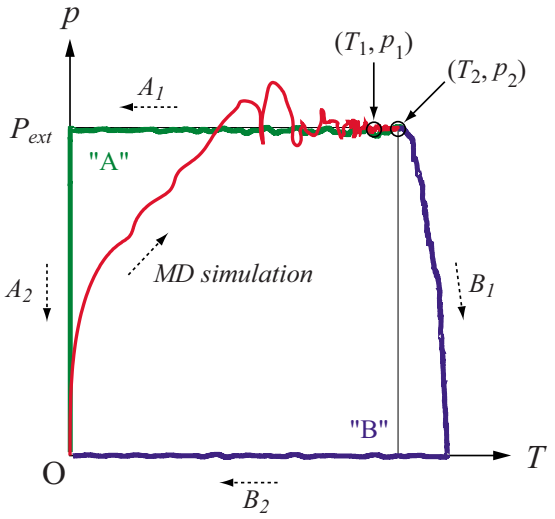

FIG. 2. (Color online) Trajectory of (T,p) in the MD simulation process for $P_{\text{ext}}=20$ GPa. The final T and p values after 2000 steps, (T_2,p_2), as well as their values at 1200 steps, (T_1,p_1), are indicated by open circles. It is evident that p_1 is already almost equal to P_{ext}, and T_1 is also very close to the final value, T_2 (941 K in this case). In the two different ways (A and B, see text) of studying the stability of the final structure under ambient pressure and low temperature, T and p values change along the trajectories A_1+A_2 and B_1+B_2 for processes A and B, respectively. In process B after switching the target pressure from P_{ext} to zero, potential energy is partly converted to the kinetic energy and the temperature of the system gradually increases (trajectory B_1).

$$T = \left\langle \frac{2}{3Nk} \sum_{i=1}^{N} \frac{m}{2} \boldsymbol{v}_i^{\mathrm{T}} \boldsymbol{v}_i \right\rangle, \tag{3}$$

where N is the total number of atoms in the MD cell (120 in the present work), and k and m are, respectively, the Boltzmann constant and the averaged mass of a carbon atom with the natural abundance of ^{12}C and ^{13}C. It is evident that the present simulation of 2000 MD steps is long enough to reach the equilibrium under the given P_{ext}. In Fig. 2, T and p values during the processes A and B are also shown.

III. RESULTS AND DISCUSSION

A. Molecular-dynamics study

During the constant-pressure MD simulation, it is found that as soon as the external pressure is applied, 2D polymerized C_{60} planes approach each other and the value of a_3 becomes small. In the simulation of $P_{\text{ext}}=10$ GPa, for example, the value of a_3 becomes as short as 12.09 Å. However, the C-C bond network remains the same throughout the entire MD simulation process. On the other hand, in the simulation of $P_{\text{ext}}=12$ GPa or higher, chemical bonds between C_{60} planes are formed immediately after the interlayer distance becomes shorter than some critical values, and transformation to a 3D network structure is completed at the relatively early stage (~0.2 ps) of the whole simulation time. Interestingly, the critical value of a_3 for 3D network formation is found to depend on P_{ext}; 12.86 Å for $P_{\text{ext}}=12$ GPa and 13.27 Å for $P_{\text{ext}}=30$ GPa.

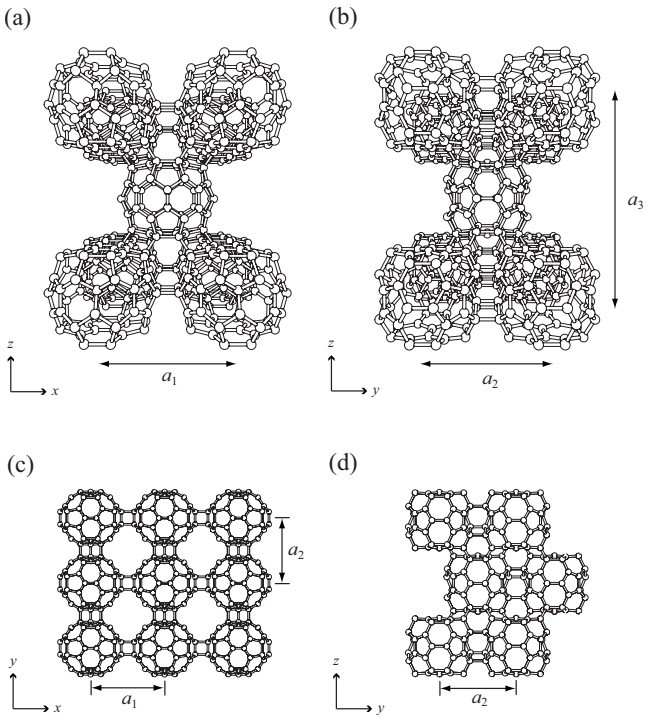

FIG. 3. Schematic picture of three-dimensionally polymerized C_{60} phase at $p=0$ and $T=0$ viewed from (a) y and (b) x directions, respectively. The geometry is obtained via process A after the constant-pressure MD simulation of 20 GPa. (c) C_{60} units on the initial two-dimensional polymer plane. Although there are five interfullerene bonds along the $y(a_2)$ direction, two of them are overlapping with other bonds in this figure and do not show up. (d) Similarly, the side view of this complex interfullerene bonding along the y direction, where only three bonds show up again. It is apparent from (d) that there are two kinds of this complex interfullerene bonding along the y direction although they are mirror symmetric to each other with respect to the xy plane. Therefore, the material possesses not the body-centered-orthorhombic unit cell but the orthorhombic primitive unit cell.

The 3D polymer geometry obtained is found to be preserved in the rest of the "long" MD simulation process. Up to 28 GPa, surprisingly, the results are mostly the same and the 3D polymer phase is always obtained. However, in the simulation of $P_{\text{ext}}=30$ GPa, the final structure eventually becomes not a C_{60} polymer phase but the strongly distorted phase where the original topological network of C atoms in C_{60} has been altered considerably. In all the MD simulations where transformation to a 3D polymer phase takes place, the temperature of the system gradually goes up until the reaction is completed, and eventually reaches the final value of about 600 K ($P_{\text{ext}}=12$ GPa) to 1500 K ($P_{\text{ext}}=28$ GPa).

We next check the structural stability of the 3D polymer by using both procedure A and B. Although the lattice constants of the system is found to be elongated when the pressure is released and the system is cooled, the 3D polymerized geometry obtained under pressure is found to be stable. In Fig. 3, we show the structure of the 3D polymer phase obtained under the external pressure of 20 GPa and subsequent pressure releasing and cooling by procedure A. This structure possesses the orthorhombic primitive geometry. The lattice

constants a_1, a_2, and a_3 are 8.90, 7.84, and 12.86 Å, respectively. Interestingly, these values are very close to those of the experimentally synthesized material by Yamanaka *et al.*,[15] a_1=8.59, a_2=7.86, and a_3=12.73 Å.

On the other hand, interfullerene covalent-bond network obtained in the present MD simulation is found to be different from that of experimentally proposed geometry. Although the four-membered ring initially connecting fullerenes along the $x(a_1)$ direction is preserved in the 3D polymer, the four-membered ring initially connecting fullerenes along $y(a_2)$ direction is now replaced by a more complex bonding pattern with five interfullerene bonds. In addition, each C_{60} unit possesses two interfullerene bonds with all the eight remaining neighbor C_{60} fullerenes via [3+3] cycloaddition. Therefore, in the present 3D C_{60} polymer phase, each C_{60} is completely polymerized with 12 C_{60} neighbors. In the experimental geometry,[15] however, each C_{60} unit possesses interfullerene bonds only with its eight neighbor C_{60} fullerenes via [3+3] cycloaddition.

The complex interfullerene bonding pattern along the a_2 direction discussed above is found to show even more variations depending on the value of the external pressure P_{ext} as well as the way of removing temperature and pressure (processes A or B). Figure 4 shows all the bonding patterns which have appeared in the a_2-axis direction. At the initial 2D polymer, a four-membered ring with two interfullerene bonds is formed. However, in the 3D polymer phases obtained, it is found that this four-membered ring is not necessarily stable. In Figs. 4(a), 4(b), 4(e), and 4(f), one of the two interfullerene bonds is broken, and both are broken in Fig. 4(d). On the other hand, it is also found that interfullerene bonds between the atoms which are the nearest-neighbor atoms of the initial four-membered-ring atoms are newly formed. In most cases, all these four nearest-neighbor atoms possess interfullerene bonds [(a) to (d)], while in some exceptional cases, three nearest-neighbor atoms possess interfullerene bonds. Interestingly, it is found that the process A always gives rise to the phases with either only pattern (a) or the combination of (a) and (b) independently of the value of P_{ext}, corresponding to the bco and the orthorhombic primitive lattice, respectively. On the other hand, process B yields patterns (c)–(f) in addition to patterns (a) and (b). Among these four additional patterns, pattern (c) appears rather frequently for P_{ext}=12, 14, 24, and 28 GPa.

As can be expected from the fact that patterns (a) and (b) are most frequently observed at p=0 and T=0, the 3D polymer geometry with both patterns (a) and (b) (Fig. 3) is found to be the lowest-energy geometry within the TB model. Also the bco 3D polymer with pattern (a) is found to be slightly higher in energy only by 0.8 meV per atom. Other 3D-polymer phases with patterns (c), (d), (e), or (f) is energetically higher, although even the highest-energy phase has the energy which is higher only by 9.1 meV per atom than the lowest-energy geometry. Therefore, in order to predict the interfullerene bonding pattern along the a_2 axis more precisely, we next perform the LDA geometry optimization.

B. DFT-LDA study

Among the 3D polymer phases obtained, we study the bco phase in LDA in order to check the stability of the most typical pattern (a) with as high accuracy as possible. In the geometry optimization, we assume that each C_{60} unit maintains the point-group symmetry of C_{2v}. This symmetry is retained not only in the bco phase but also in the orthorhombic primitive phase obtained via TBMD calculation. As for the k-point sampling, 27 points in the whole Brillouin zone are used.

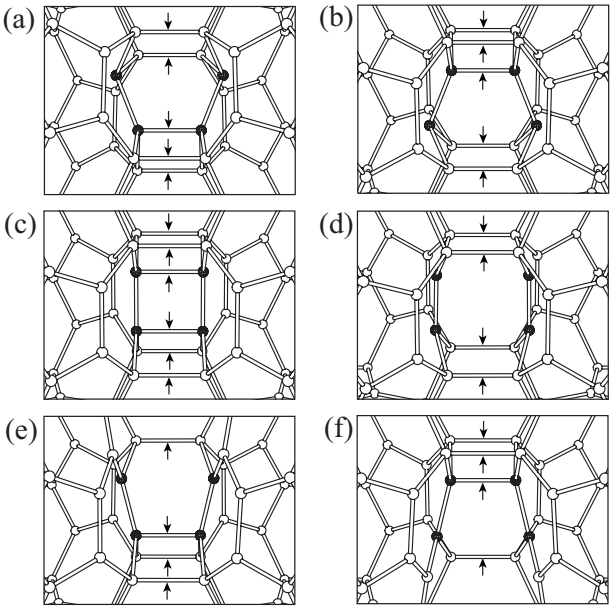

FIG. 4. A variety of interfullerene bonding patterns that appear in the $\boldsymbol{a}_2$ direction. In each panel, the horizontal direction corresponds to the direction of $\boldsymbol{a}_2$. In order to avoid the overlapping of bonds and to show the number of interfullerene bonds clearly, the line of sight is set to be slightly above the $\boldsymbol{a}_1$ axis in each panel except in panel (a) where the line of sight is slightly below the $\boldsymbol{a}_1$ axis. Arrows indicate the interfullerene bonds, and decorated spheres represent the atoms on the four-membered ring at the initial two-dimensional phase. Patterns (a) and (b) are essentially the same but they should be distinguished if both appear simultaneously as in the case of P_{ext}=20 GPa and process A [Fig. 3(d)]. Patterns (e) and (f) are also the same as in the case of (a) and (b). Therefore, patterns (a) and (c)–(e) are the main different patterns obtained in the present TBMD simulation.

The optimized geometry in LDA is found to possess almost the same network topology as that of the TB calculation. In the LDA geometry, importantly, 90 intrafullerene bonds of each C_{60} all remain connected. Also, the two interfullerene bonds in the diagonal direction and the four-membered ring in the direction of $\boldsymbol{a}_1$ are found to be preserved. However, as for the direction of $\boldsymbol{a}_2$, the bonding pattern is found to be not (a) but (d) in Fig. 4. This result suggests that the pattern (d) is much more stable than other patterns in LDA because one can obtain all the other three patterns [(c)–(e)] from the pattern (a) by just connecting or breaking one bond. The LDA energetics reveals that the pattern (a) should automatically change into the pattern (d), which indicates that the pattern (d) may be the most stable pattern among all the patterns obtained in the TBMD simulation. Therefore, the most stable phase in LDA should possess not the orthorhombic primitive but the bco geometry.

TABLE I. LDA total energies of various phases of solid C_{60} measured from the total LDA energy of graphite.

	E_{tot} (eV/atom)
Experimental model	0.551
Present work	0.495
Two-dimensional rhombohedral[a]	0.429
fcc C_{60} [a]	0.427
Two-dimensional orthorhombic[a]	0.406

[a]Reference 35.

It is interesting to note that this pattern (d) possesses the same interfullerene bonding topology as the most stable phase proposed based on the static GGA calculation.[17] However, our lattice constants are found to be considerably different from the GGA phase. After the geometry optimization, the bco 3D polymer possesses the lattice constants of a_1 =8.92, a_2=7.90, and a_3=13.00 Å. These values are all slightly longer than those in the TB geometry, and shorter than the optimized values of GGA (a_1=9.08, a_2=8.03, a_3 =13.22 Å).[17] Interestingly, it is found that the present LDA result is slightly closer to the experimental lattice-constant values[15] than the GGA. The LDA total energy of this bco phase is found to be 0.495 eV per atom higher than that of graphite (Table I). This value is 0.089 eV per atom higher than that of the 2D orthorhombic polymer phase, i.e., the initial structure of the present work. On the other hand, volume per atom of the 3D polymer phase is 7.64 Å^3, which should be definitely smaller than that of the initial 2D orthorhombic phase. Within the TB used in the present work, the volume per atom of the 2D polymer phase is 9.26 Å^3, and the experimentally reported values are 10.29 and 10.30 Å^3 in Ref. 10 and Refs. 11 and 15, respectively. Therefore, the structural phase transition from 2D to 3D polymer should automatically take place under external pressure.

For comparison, we also study the energetics of the structural model of the 3D polymer phase proposed experimentally.[15] It is found that when the internal structure of the model as well as the lattice constants is optimized in LDA, its interfullerene bonding pattern changes along the a_1 axis. In the initial geometry, i.e., the geometry of the structural model,[15] there are no interfullerene bonds in the directions of both $\boldsymbol{a}_1$ and $\boldsymbol{a}_2$, whereas in the optimized geometry, four interfullerene bonds are newly formed in the a_1-axis direction. The optimized lattice constants are a_1=8.40, a_2 =8.30, and a_3=12.94 Å. The total energy obtained for this optimized geometry is found to be higher than the initial 2D polymer by 0.145 eV per atom. This energy difference is considerably larger than the energy difference between the initial 2D phase and the completely polymerized phase with the pattern (d) found in the present work. Therefore, the present 3D polymer phase would be a stable phase to be produced from the 2D polymer phase in the future experiments.

In the MD scheme we used in this study,[22] the enthalpy of the system is conserved throughout the simulation process. Therefore, the temperature of the system goes up when the volume of the cell decreases as has been mentioned previously. Hence, simulations performed in the present work may correspond to the shock compression rather than the static slow compression as performed in the experiment.[15] This may be the reason why the present 3D polymer phase is different from the 3D polymer model proposed experimentally. On the other hand, it is well known that different structures coexist under a certain thermal condition in carbon material, e.g., graphite and diamond under ambient condition. Therefore, the energetically favorable present 3D polymer phase might be also produced even in the static-compression experiment by carefully controlling the temperature and pressure.

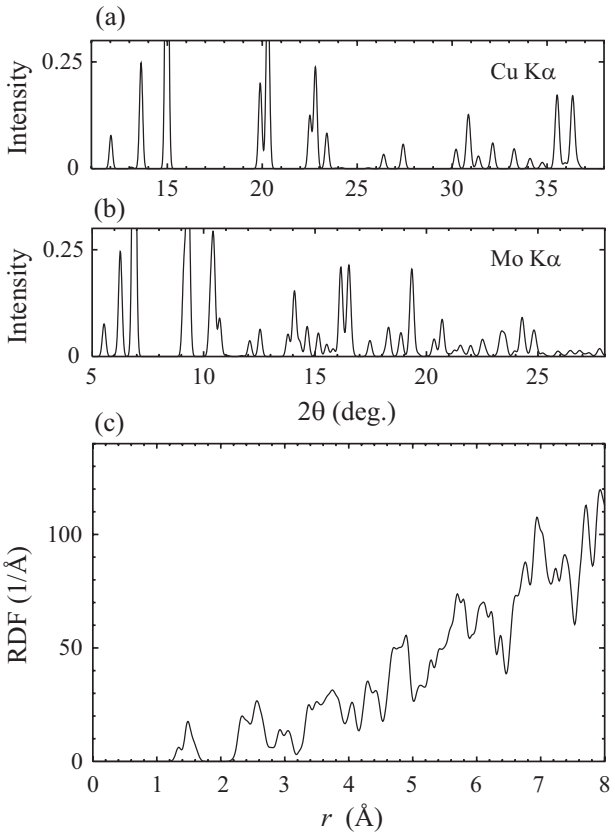

FIG. 5. (a) X-ray powder-diffraction pattern simulated for the LDA-optimized three-dimensional polymer geometry in using Cu $K\alpha$ spectral line (λ=1.540 60 Å), and (b) that using Mo $K\alpha$ spectral line (λ=0.709 26 Å). Intensity is normalized so that the third peak's top is equal to one in both (a) and (b). (c) Radial distribution function for the LDA-optimized three-dimensional polymer geometry. Broadening of peaks is expressed by a Gaussian function with a full width at half maximum of 0.96 Å.

This 3D polymer phase possesses as much as 28 sp^3 (fourfold-coordinated) C atoms, corresponding to 46.7% of all the C atoms in the phase. This ratio may be an important clue to reveal the 3D polymer structure because it can be experimentally examined by using the ^{13}C nuclear magnetic resonance (NMR). The 2D rhombohedral phase has been already examined in this way, and the value of 19.5% ± 5% is obtained,[36] which is very close to the ideal value of 20.0%. Therefore, the presence of the 3D polymer phase obtained in this work should be also verified by the ^{13}C NMR experiment if the sample contains the phase as a majority phase.

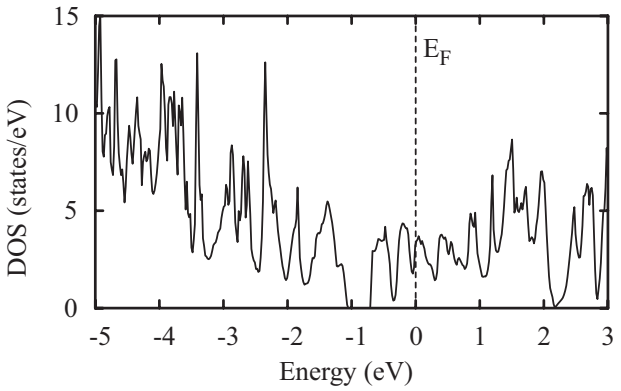

FIG. 6. LDA electronic density of states (DOS) of the 3D polymer phase. The energy is measured from the Fermi energy E_F. Interestingly, the system is metallic while a small gap of 0.34 eV opens within the valence band.

In Fig. 5, we show the simulated x-ray powder-diffraction pattern and the radial distribution function of the 3D polymer phase obtained in the present LDA geometry optimization. There are nine independent atomic sites in this geometry: (0.411, 0.096, 0.000), (0.260, 0.312, 0.056), (0.000, 0.356, 0.051), (0.340, 0.179, 0.090), (0.135, 0.397, 0.112), (0.318, 0.101, 0.194), (0.092, 0.315, 0.217), (0.157, 0.144, 0.214), and (0.078, 0.000, 0.223). These figures will be also useful in the future to verify the presence of this phase in the sample.

This half-sp^3 3D C_{60} polymer phase should have unique electronic structure which is different from other 1D/2D polymer phases. Figure 6 shows the LDA electronic density of states of this phase. Actually, as can be seen from the figure, this 3D polymer phase is found to possess metallic electronic structure. It is interesting that this phase is metallic in spite of its relatively high sp^3 ratio, although both orthorhombic and rhombohedral 2D polymer phases are revealed to be insulating in our previous work.[35] Within the valence band, the gap of 0.34 eV appears about 1 eV below the Fermi level. The depth of the valence-band bottom measured from the Fermi level is −21.35 eV, which is more than 1 eV deeper than that of graphite.[37–39]

IV. SUMMARY AND CONCLUDING REMARKS

Using the tight-binding molecular-dynamics (TBMD) method, we study the structural phase transition of the 2D orthorhombic polymer for a wide pressure range (10–30 GPa). Under the external pressure of 12–28 GPa, the 2D phase turns into almost the same 3D polymer phases, with a small variation in the interfullerene bonding along the a_2 axis. The total-energy differences between these TB phases are found to be small, of the order of 10 meV or even smaller. Actually, the LDA geometry optimization suggests that the pattern with four interfullerene bonds is the most stable pattern to be observed experimentally. Its energy per atom in the LDA is found to be relatively low. Therefore, this phase should be stable once it was synthesized. Since this 3D polymerized phase is found to be electronically conductive, the phase is an interesting target in the field of pressure synthesis of new materials.

ACKNOWLEDGMENTS

We would like to thank T. Koretsune for useful discussion. We would like to thank A. Oshiyama, T. Nakayama, M. Saito, and O. Sugino for the LDA program used in the present study. An original version of the MD program used in the present work was written by R. M. Wentzcovitch. The MD calculations were mainly performed on TSUBAME Grid Cluster at the Global Scientific Information and Computing Center of the Tokyo Institute of Technology. The LDA calculations were performed on NEC SX7 at Research Center for Computational Science, Okazaki National Institute. We also acknowledge the financial support from the Asahi Glass Foundation and the Global Center-of-Excellence Program by the Ministry of Education, Science, and Culture of Japan (MEXT) through the Nanoscience and Quantum Physics Project of the Tokyo Institute of Technology. This work is in part supported by a Grant-in-aid for Scientific Research by MEXT under Contracts No. 19054005 and No. 18204033.

[1] W. Krätschmer, L. D. Lamb, K. Fostiropoulos, and D. R. Huffman, Nature (London) **347**, 354 (1990).
[2] S. Saito and A. Oshiyama, Phys. Rev. Lett. **66**, 2637 (1991).
[3] J. H. Weaver, J. L. Martins, T. Komeda, Y. Chen, T. R. Ohno, G. H. Kroll, N. Troullier, R. E. Haufler, and R. E. Smalley, Phys. Rev. Lett. **66**, 1741 (1991).
[4] R. C. Haddon, A. F. Hebard, M. J. Rosseinsky, D. W. Murphy, S. J. Duclos, K. B. Lyons, B. Miller, J. M. Rosamilia, R. M. Fleming, A. R. Kortan, S. H. Glarum, A. V. Makhija, A. J. Muller, R. H. Eick, S. M. Zahurak, R. Tycko, G. Dabbagh, and F. A. Thiel, Nature (London) **350**, 320 (1991).
[5] A. F. Hebard, M. J. Rosseinsky, R. C. Haddon, D. W. Murphy, S. H. Glarum, T. T. M. Palstra, A. P. Ramirez, and A. R. Kortan, Nature (London) **350**, 600 (1991).
[6] K. Tanigaki, T. W. Ebbesen, S. Saito, J. Mizuki, J. S. Tsai, Y. Kubo, and S. Kuroshima, Nature (London) **352**, 222 (1991).
[7] A. M. Rao, P. Zhou, K.-A. Wang, G. T. Hager, J. M. Holden, Y. Wang, W.-T. Lee, X.-X. Bi, P. C. Eklund, D. S. Cornett, M. A. Duncan, and I. J. Amster, Science **259**, 955 (1993).
[8] Y. Iwasa, T. Arima, R. M. Fleming, T. Siegrist, O. Zhou, R. C. Haddon, L. J. Rothberg, K. B. Lyons, H. L. Carter, Jr., A. F. Hebard, R. Tycko, G. Dabbagh, J. J. Krajewski, G. A. Thomas, and T. Yagi, Science **264**, 1570 (1994).
[9] C. H. Xu and G. E. Scuseria, Phys. Rev. Lett. **74**, 274 (1995).
[10] M. Núñez-Regueiro, L. Marques, J.-L. Hodeau, O. Béthoux, and M. Perroux, Phys. Rev. Lett. **74**, 278 (1995).
[11] X. Chen and S. Yamanaka, Chem. Phys. Lett. **360**, 501 (2002).
[12] S. Okada, S. Saito, and A. Oshiyama, Phys. Rev. Lett. **83**, 1986 (1999).
[13] L. A. Chernozatonskii, N. R. Serebryanaya, and B. N. Mavrin,

Chem. Phys. Lett. **316**, 199 (2000).
[14] D. H. Chi, Y. Iwasa, T. Takano, T. Watanuki, Y. Ohishi, and S. Yamanaka, Phys. Rev. B **68**, 153402 (2003).
[15] S. Yamanaka, A. Kubo, K. Inumaru, K. Komaguchi, N. S. Kini, T. Inoue, and T. Irifune, Phys. Rev. Lett. **96**, 076602 (2006).
[16] S. Yamanaka, N. S. Kini, A. Kubo, S. Jida, and H. Kuramoto, J. Am. Chem. Soc. **130**, 4303 (2008).
[17] F. Zipoli and M. Bernasconi, Phys. Rev. B **77**, 115432 (2008).
[18] P. Hohenberg and W. Kohn, Phys. Rev. **136**, B864 (1964).
[19] W. Kohn and L. J. Sham, Phys. Rev. **140**, A1133 (1965).
[20] S. Nosé, Mol. Phys. **52**, 255 (1984).
[21] V. R. Coluci, F. Sato, S. F. Braga, M. S. Skaf, and D. S. Galvão, J. Chem. Phys. **129**, 064506 (2008).
[22] M. Parrinello and A. Rahman, Phys. Rev. Lett. **45**, 1196 (1980).
[23] C. H. Xu, C. Z. Wang, C. T. Chan, and K. M. Ho, J. Phys.: Condens. Matter **4**, 6047 (1992).
[24] Y. Omata, Y. Yamagami, K. Tadano, T. Miyake, and S. Saito, Physica E **29**, 454 (2005).
[25] A. N. Kolmogorov and V. H. Crespi, Phys. Rev. B **71**, 235415 (2005).
[26] J. W. McClure, Phys. Rev. **108**, 612 (1957).
[27] J. C. Slonczewski and P. R. Weiss, Phys. Rev. **109**, 272 (1958).
[28] J. W. McClure, Phys. Rev. **119**, 606 (1960).
[29] N. Troullier and J. L. Martins, Phys. Rev. B **43**, 1993 (1991).
[30] L. Kleinman and D. M. Bylander, Phys. Rev. Lett. **48**, 1425 (1982).
[31] D. M. Ceperley and B. J. Alder, Phys. Rev. Lett. **45**, 566 (1980).
[32] J. P. Perdew and A. Zunger, Phys. Rev. B **23**, 5048 (1981).
[33] O. Sugino and A. Oshiyama, Phys. Rev. Lett. **68**, 1858 (1992).
[34] We have also tried much lighter W value (35 times the proton mass) for some cases but results obtained are found to remain unchanged.
[35] S. Okada and S. Saito, Phys. Rev. B **59**, 1930 (1999).
[36] Y. Maniwa, M. Sato, K. Kume, M. E. Kozlov, and M. Tokumoto, Carbon **34**, 1287 (1996).
[37] P. Zhang, S. Saito, S. G. Louie, and M. L. Cohen, Phys. Rev. B **77**, 052501 (2008).
[38] H. J. F. Jansen and A. J. Freeman, Phys. Rev. B **35**, 8207 (1987).
[39] J. C. Boettger, Phys. Rev. B **55**, 11202 (1997).